

Reconciling spectroscopy with dynamics in global potential energy surfaces: the case of the astrophysically relevant SiC₂

C. M. R. Rocha*,¹ H. Linnartz,¹ and A. J. C. Varandas^{2,3,4}

¹*Laboratory for Astrophysics, Leiden Observatory, Leiden University, P.O. Box 9513, NL-2300 RA Leiden, The Netherlands*

²*School of Physics and Physical Engineering, Qufu Normal University, 273165 Qufu, China*

³*Department of Physics, Universidade Federal do Espírito Santo, 29075-910 Vitória, Brazil*

⁴*Department of Chemistry, and Chemistry Centre, University of Coimbra, 3004-535 Coimbra, Portugal*

(*Electronic mail: romerorocha@strw.leidenuniv.nl.)

(Dated: 11 August 2022)

SiC₂ is a fascinating molecule due to its unusual bonding and astrophysical importance. In this work, we report the first global potential energy surface (PES) for ground-state SiC₂ using the combined-hyperbolic-inverse-power-representation (CHIPR) method and accurate *ab initio* energies. The calibration grid data is obtained via a general dual-level protocol developed afresh herein that entails both coupled-cluster and multireference configuration interaction energies jointly extrapolated to the complete basis set limit. Such an approach is specially devised to recover much of the spectroscopy from the PES, while still permitting a proper fragmentation of the system to allow for reaction dynamics studies. Besides describing accurately the valence strongly-bound region that includes both the cyclic global minimum and isomerization barriers, the final analytic PES form is shown to properly reproduce dissociation energies, diatomic potentials, and long-range interactions at all asymptotic channels, in addition to naturally reflect the correct permutational symmetry of the potential. Bound vibrational state calculations have been carried out, unveiling an excellent match of the available experimental data on *c*-SiC₂(¹A₁). To further exploit the global nature of the PES, exploratory quasi-classical trajectory calculations for the endothermic C₂+Si → SiC+C reaction are also performed, yielding thermalized rate coefficients for temperatures up to 5000 K. The results hint for the prominence of this reaction in the innermost layers of the circumstellar envelopes around carbon-rich stars, thence conceivably playing therein a key contribution to the gas-phase formation of SiC, and eventually, solid SiC dust.

I. INTRODUCTION

Silicon dicarbide, SiC₂, has enjoyed a great deal of attention for its applications in astrochemistry^{1–14}:

- (i). Its most stable cyclic C_{2v} isomer, *c*-SiC₂(¹A₁), was the first molecular ring identified in the interstellar medium¹.
- (ii). Its Merrill-Sanford band system ($\tilde{A}^1B_2-\tilde{X}^1A_1$ electronic transition) near 5000 Å was first observed in the optical absorption spectra of evolved stars, and continues to be a particularly valuable astronomical probe of stellar atmospheres^{4,5}.
- (iii). Besides rovibronic transitions, the pure rotational signatures of both main (²⁸Si¹²C₂) and singly-substituted isotopologues (²⁹SiC₂, ³⁰SiC₂, and ²⁸Si¹³CC) of *c*-SiC₂ have been identified in several astrophysical sources^{1,2,6–8,10,11} and serve as sensitive molecular diagnostic tools for probing the chemical and physical conditions of the regions in which they reside^{1,6}.
- (iv). Together with SiC and Si₂C parent molecules, *c*-SiC₂ is ranked among the most likely gas-phase precursors leading to the formation of SiC dust grains in the inner envelopes of late-type carbon-rich stars^{9,10,12,13}.

Apart from its intrinsic interest in an astronomical context, SiC₂ is also a fascinating molecule from a chemical viewpoint

owing to its unique structure and dynamics^{15,16}. Previous laboratory^{15,17,18} and quantum mechanical studies^{16,19–21} jointly provided ample evidence that its lowest energy C_{2v} minimum (as definitively assigned by Michalopoulos *et al.*¹⁷) has an exceedingly flat potential energy surface (PES) along the internal rotation of the C₂ moiety within the molecule^{15–21}. Such an untypical, nondirectional Si–C₂ bonding in *c*-SiC₂ (with reportedly high ionic character) has been classified^{16,22} as polytopic²³ in nature, and hence characterized by the nearly-free circumnavigation of Si about C₂²³. Indeed, the expectedly low energy difference between *c*-SiC₂ and the linear C_{∞v} (*ℓ*-SiCC) saddle-point structure was first confirmed experimentally by Ross *et al.*¹⁵ as being only ~1883 cm^{–1}. Clearly, like in C₃^{24,25}, the expected high vibrational state populations and their delocalization over large regions of the PES make *c*-SiC₂'s intramolecular motion lying at the borderlines of spectroscopy and chemical dynamics.

The conclusions drawn from these early experimental works by Michalopoulos *et al.*¹⁷ and Ross *et al.*¹⁵ motivated a plethora of detailed spectroscopic studies on *c*-SiC₂ aiming to further characterize its spectral signatures in both microwave^{7,8,11,12,26}, infrared^{27–29} and optical^{18,30} regions; for a comprehensive review, see Ref. 30 and references therein.

From the theoretical perspective, several concurring investigations were also ignited towards unraveling the SiC₂'s unusual polytopic bonding nature and its large-amplitude dynamics^{16,19–22,31–33}; for a complete account of the earlier theo-

retical literature the reader is addressed to Refs. 16 and 21. In the most recent studies by Fortenberry *et al.*²⁰ and Koput²¹, special emphasis were put into the characterization of the *c*-SiC₂'s local PES using state-of-the-art *ab initio* composite methods. By relying on the so-called CcCR protocol²⁰, Fortenberry *et al.* reported a near-equilibrium quartic force field (QFF) for silicon dicarbide; the QFF was based on CCSD(T) energies extrapolated to the complete basis set (CBS) limit, augmented by additive corrections due to core-electron correlation and relativistic effects²⁰. Using standard vibrational perturbational theory (VPT2), the CcCR QFF has shown to reproduce the *c*-SiC₂'s stretching fundamentals (ν_1 and ν_2) to within 5 cm⁻¹ of experiment¹⁸, whereas larger deviations of up to 21 cm⁻¹ have been found for the ν_3 (C₂ hindered rotation) mode²⁰. As noted by Nielsen *et al.*¹⁶ and Koput²¹, this is not surprising given the inherent deficiencies of VPT2 in properly describing such highly-anharmonic, large-amplitude pinwheel dynamics of *c*-SiC₂. In the most sophisticated theoretical study to date by Jacek Koput²¹, a more extended PES (hereinafter referred to as JK PES) was reported that describes locally not only *c*-SiC₂ but also the ℓ -SiCC saddle-point, in addition to the minimum energy path connecting them; the calibration data set included *ab initio* CCSD(T)-F12b/cc-pCVQZ-F12 energies additively corrected for higher-order valence-electron correlation beyond CCSD(T) and scalar relativistic effects²¹. Its barrier to linearity was predicted to be 1782 cm⁻¹ which is lower than the previous high-level *ab initio* estimates by Nielsen *et al.*¹⁶ (2030 cm⁻¹), and Kenny *et al.*¹⁹ (2210 cm⁻¹), but closer to the experimental value¹⁵ of 1883 cm⁻¹. Based on a variational approach, Koput²¹ also performed bound-state calculations on his final potential; the results have shown that the JK PES is capable of reproducing the *c*-SiC₂'s experimental vibrational term values reported by Ross *et al.*¹⁵ with a root-mean-square deviation (rmsd) of ~ 5 cm⁻¹.

Clearly, all the above distinctive features of SiC₂ make it a challenging testing ground for any theoretical methodological development. Moreover, the expected implications its unique spectroscopy and reaction dynamics might have in molecular astrophysics, render this molecule a tempting target for further studies. As noted above, previous theoretical studies were mainly concerned with the determination of locally valid spectroscopic potentials for *c*-SiC₂^{16,20,21} and there is not as yet a global PES for the title system that is capable of accurately describing both its valence and dissociation features at once. In this work, we delve deeper into the silicon dicarbide saga¹⁶ and provide for the first time such a form for ground-state SiC₂. To allow for both bound-state and reaction dynamics calculations, the PES will be based on an accurate *ab initio* protocol that incorporates the best of two worlds: coupled-cluster [CCSD(T)] and multireference configuration interaction [MRCI(Q)] energies jointly extrapolated to the CBS limit. For the analytical modeling, we employ the Combined-Hyperbolic-Inverse-Power-Representation (CHIPR) method³⁴⁻³⁷ as implemented in the CHIPR-4.0 program³⁷. The quality of the final potential is further judged via both spectroscopic and exploratory reaction dynamics calculations.

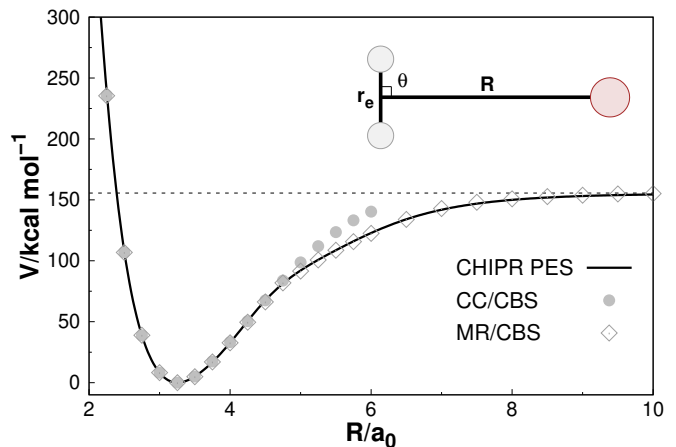


FIG. 1. Extrapolated CCSD(T) [CC/CBS] and MRCI(Q) [MR/CBS] energies for a cut along the perpendicular ($\theta = 90^\circ$) approach of a Si atom into the C₂ diatomic with $r_e = 2.40133 a_0$. The corresponding final CHIPR PES is also shown for comparison. The zero of energy corresponds to the T-shaped (C_{2v}) global minimum at $R = 3.25350 a_0$.

II. METHODOLOGY

A. *Ab initio* calculations

All electronic structure calculations have been done with MOLPRO³⁸. To ensure an accurate description of both valence and long-range features of the PES, the full set of *ab initio* grid points were herein generated using a combination³⁹ of CCSD(T)⁴⁰⁻⁴² (CC for brevity) and MRCI(Q)⁴³ (MR) levels of theory. The first is specially devised to improve the spectroscopy of the global minimum and is limited [due to the well-known^{39,43} erratic behaviour of such single-reference method for stretched bond distances (Figure 1)] to a small region of the PES near the *c*-SiC₂/ ℓ -SiCC stationary points. The MR set is in turn responsible to cover the bulk of the PES⁴³, being restricted to sample the fragmentation region and geometries with high T_1 and D_1 diagnostics^{44,45} [*e.g.*, those characterized by larger C–C bond distances, away from the equilibrium region; see Figure 3(a) later]. Both data sets were subsequently extrapolated to the CBS limit^{46,47} (see below). The AVXZ ($X = T, Q, 5$) basis sets of Dunning and co-workers^{48,49} including additional tight-*d* functions (+*d*) for the Si atom³⁸ were employed throughout.

At each selected geometry \mathbf{R} , the CC/CBS energy was defined as⁵⁰

$$E_\infty^{\text{CC}}(\mathbf{R}) = E_\infty^{\text{HF}}(\mathbf{R}) + E_\infty^{\text{cor}}(\mathbf{R}), \quad (1)$$

where E_∞^{HF} and E_∞^{cor} are the extrapolated HF and CC correlation (cor) components. In Eq. (1), E_∞^{HF} is obtained via a two-point extrapolation protocol⁵¹

$$E_X^{\text{HF}}(\mathbf{R}) = E_\infty^{\text{HF}}(\mathbf{R}) + A e^{-\beta x} \quad (2)$$

where $x = q(3.87)$, $p(5.07)$ are hierarchical numbers^{52,53} that parallel the traditional $X = Q, 5$ cardinal ones, $\beta = 1.62$, and E_∞^{HF} and A are parameters to be calibrated from the raw

RHF/AVXZ ($X = Q, 5$) energies⁵¹. In turn, E_{∞}^{cor} is obtained using the inverse-power formula⁵²

$$E_X^{\text{cor}}(\mathbf{R}) = E_{\infty}^{\text{cor}}(\mathbf{R}) + \frac{A_3}{x^3}, \quad (3)$$

where $q(3.68)$, $p(4.71)$ are CC-type x numbers⁵², with E_{∞}^{cor} and A_3 calibrated from the raw CC/AVXZ ($X = Q, 5$) cor energies.

Similarly to Eq. (1), the CBS extrapolations of MR energies were performed individually for the non-dynamical (CAS) and dynamical (dc) correlations⁵⁴

$$E_{\infty}^{\text{MR}}(\mathbf{R}) = E_{\infty}^{\text{CAS}}(\mathbf{R}) + E_{\infty}^{\text{dc}}(\mathbf{R}), \quad (4)$$

where E_{∞}^{CAS} is obtained using Eq. (2) but with CASSCF(12,12)/AVXZ ($X = T, Q$) raw energies⁵¹ and E_{∞}^{dc} is given by the two-point law⁵⁵

$$E_X^{\text{dc}}(\mathbf{R}) = E_{\infty}^{\text{dc}}(\mathbf{R}) + \frac{A_3}{(X-3/8)^3} + \frac{A_5^0 + cA_3^{5/4}}{(X-3/8)^5}; \quad (5)$$

here, A_5^0 and c are universal-type parameters⁵⁵, and E_{∞}^{dc} and A_3 are obtained from the raw MRCI(Q)/AVXZ ($X = T, Q$) dc energies. The full-valence CASSCF active space includes the 3s- and 3p-like orbitals of Si and the 2s- and 2p-like orbitals of the C atoms. Note that, in the CC calculations, core correlation was not taken into account as this would imply, for reasons of consistency between both data sets, the consideration of such effects also at MR level, making the task of obtaining the global PES computationally unaffordable with current available resources. Thus, in all CC and MR calculations, only the valence electrons were correlated, with the 2s- and 2p-like orbitals of Si being included into the core.

Using the above dual-level CC/MR CBS protocol, a total of 3682 symmetry unique points (1144 and 2538 at CC/CBS and MR/CBS levels, respectively) have been selected to map all relevant regions of the ground-state PES of SiC₂ using atom-diatom Jacobi coordinates⁵⁶ (r , R , and θ in Figure 1); the ranges are $2.0 \leq R/a_0 \leq 15.0$, $2.0 \leq r/a_0 \leq 3.5$, and $0.0 \leq \theta/\text{deg} \leq 90.0$ for the Si-C₂ channel and $1.2 \leq R/a_0 \leq 15.0$, $2.8 \leq r/a_0 \leq 4.3$, and $0.0 \leq \theta/\text{deg} \leq 180.0$ for C-SiC interactions. Recall that, in partitioning the nuclear configuration space, the CC/CBS data set was chosen to cover only a limited region around the global minimum (including ℓ -SiCC), while the MR/CC method was utilized elsewhere. Note that the corresponding C₂ and SiC curves were obtained solely at the MR/CBS level by making atom-diatom calculations with the Si and C atoms $50a_0$ far apart, varying the diatomic internuclear distance only; the total number of computed points for each curve amounts to ~ 63 and covers the coordinate range of $1.0 \leq r/a_0 \leq 50$. The reader is addressed to Figure 3(a) and Figures S1 and S2 of the Supplementary Material (SM) to assess the full set of *ab initio* grid points.

Finally, it should be noted that, while the use of larger basis sets would be desirable in estimating the CBS limits in Eqs. (1)-(5), preliminary test calculations have shown that the associated computational cost to obtain the full global PES would be nearly three times as high if the cardinal numbers in the above extrapolation formulas were increased by one unit. Because our proposed MR/CBS(T, Q)

TABLE I. Stratified root-mean-square deviations (in kcal mol⁻¹) of the final PES.

Energy ^a	N^b	max. dev. ^c	rmsd	$N_{>\text{rmsd}}^d$
50	804	1.5	0.2	156
100	1102	3.0	0.3	179
150	2088	3.5	0.5	249
200	2723	5.0	0.8	453
250	3430	5.1	0.9	588
500	3578	5.1	0.9	658
1200	3682	5.1	0.9	680

^a The units of energy are kcal mol⁻¹. Energy strata defined with respect to the C_{2v} absolute minimum of SiC₂: $-364.993433 E_h$ at CCSD(T)/CBS level. Its relative energy (as predicted from the PES with respect to the infinitely separated C+C+Si atoms) is $-0.474269 E_h$.

^b Number of calculated points up to indicated energy range.

^c Maximum deviation up to indicated energy range.

^d Number of calculated points with an energy deviation larger than the rmsd.

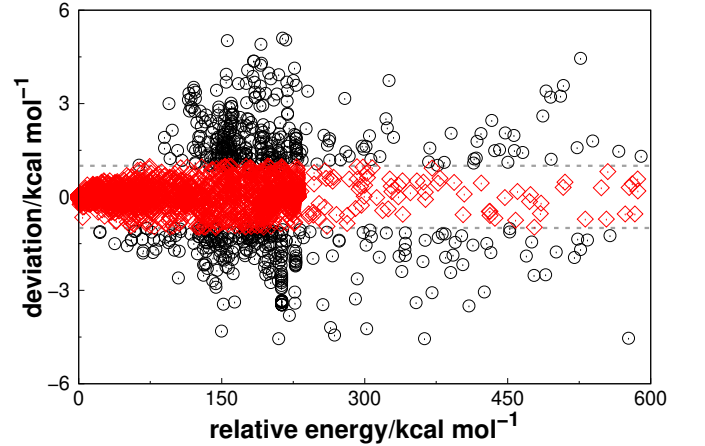


FIG. 2. Scatter plot of deviations between fitted [using the CHIPR model function of Eq. (6)] and calculated *ab initio* energies as a function of the total energy. In the x-axis, the zero is set relative to the C_{2v} global minimum of SiC₂. Points fitted with chemical accuracy ($|\text{deviation}| \leq 1 \text{ kcal mol}^{-1}$) are represented in red.

and CC/CBS($Q, 5$) protocols have already shown excellent performances when assessed against benchmark CBS energies^{46,47,51-53,55}, we deemed that there was no reason to extend the one-particle bases further.

B. Calibration of CHIPR PES

Within the CHIPR³⁴⁻³⁷ formalism, the global adiabatic PES of ground-state SiC₂(¹A') assumes the following many-body expansion form⁵⁶

$$V(\mathbf{R}) = V_{\text{C}_2}^{(2)}(R_1) + V_{\text{SiC}}^{(2)}(R_2) + V_{\text{SiC}}^{(2)}(R_3) + V_{\text{SiC}_2}^{(3)}(\mathbf{R}), \quad (6)$$

where the $V^{(2)}$'s represent the diatomic (two-body) potentials of C₂($a^3\Pi_u$) and SiC($X^3\Pi$) and $V^{(3)}$ is the three-body

term; $\mathbf{R} = \{R_1, R_2, R_3\}$ is the set of interatomic separations, with the energy zero set to the infinitely separated $C(^3P) + C(^3P) + Si(^3P)$ atoms. As Eq. (6) indicates, our analytic CHIPR PES dissociates adiabatically into $C_2(a^3\Pi_u) + Si(^3P)$ and $SiC(X^3\Pi) + C(^3P)$, thence modeling only the lowest electronic singlet state of SiC_2 correlating to such open shell fragments; this is warranted by including in Eq. (6) the proper diatomic two-body terms and ensuring that $V^{(3)}$ naturally vanishes for large interatomic separations^{36,37}. Note that, similarly to C_3 ^{24,25}, the ground-state singlet PES of SiC_2 does not dissociate adiabatically into ground-state $C_2(X^1\Sigma_g^+) + Si(^3P)$ fragments which, according to spin-correlation rules⁵⁷, correlate with the triplet manifold of SiC_2 states; see Figure S3 for further details. Note further that the spin-allowed $C_2(X^1\Sigma_g^+) + Si(^1D)$ channel lies^{58,59} $\approx 16 \text{ kcal mol}^{-1}$ above the $C_2(a^3\Pi_u) + Si(^3P)$ asymptote and correlates with excited singlet PESs^{24,25}.

In Eq. (6), the CHIPR diatomic curves are expressed by the general form³⁷

$$V^{(2)}(R) = \frac{Z_A Z_B}{R} \sum_{k=1}^L C_k y^k, \quad (7)$$

where Z_A and Z_B denote the nuclear charges of atoms A and B and the C_k 's are expansion coefficients; the y coordinate is herein defined as a linear combination of R -dependent basis functions³⁷ (see Eq. (9) below). In turn, $V^{(3)}$ in Eq. (6) is represented via CHIPR's three-body model which for AB_2 -type species assumes the simplified form^{35,37,61}

$$V^{(3)}(\mathbf{R}) = \sum_{i,j,k=0}^L C_{i,j,k} \left[y_1^i (y_2^j y_3^k + y_2^k y_3^j) \right]. \quad (8)$$

In the above equation, $C_{i,j,k}$ are expansion coefficients of a L^{th} -degree polynomial, and the y_p 's ($p = 1, 2, 3$) are (transformed) coordinates. These latter are expressed in terms of distributed-origin constructed basis sets³⁷

$$y_p = \left(\sum_{\alpha=1}^{M-1} c_{\alpha} \phi_{p,\alpha}^{[1]} \right) + c_M \phi_{p,M}^{[2]}, \quad (9)$$

where

$$\phi_{p,\alpha}^{[1]} = \text{sech} \left[\xi_{p,\alpha} (R_p - R_{p,\alpha}^{\text{ref}}) \right], \quad (10)$$

and

$$\phi_{p,M}^{[2]} = \left[\frac{\tanh(\frac{1}{5} R_p)}{R_p} \right]^6 \text{sech} \left[\xi_{p,M} (R_p - R_{p,\alpha}^{\text{ref}}) \right] \quad (11)$$

are primitive bases with origin at R^{ref} and the ξ 's are non-linear parameters. All steps involved in the calibration of Eqs. (7)-(11) using *ab initio* data points are fully described in Refs. 36 and 37, with the reader being addressed to them for further details. Note that, to obtain the global analytic form of the PES [Eq. (6)], we herein employ the newly-developed

CHIPR-4.0 program³⁷. With this code, the final CHIPR diatomic potentials of C_2 and SiC [Eq. (7)] were calibrated using MR/CBS points with rmsds of 1.1 and 0.3 cm^{-1} , respectively. For completeness, they are plotted in Figure S1. As for the three-body term, all 3682 *ab initio* dual-level CC/MR CBS points could be least-squares fitted to Eq. (8) with chemical accuracy ($\text{rmsd} = 0.9 \text{ kcal mol}^{-1}$). The weights (W) so employed were: $W = 1$ for calculated points with energies $E \leq 50 \text{ kcal mol}^{-1}$ above the global C_{2v} minimum, $W = 0.7$ for those within the interval $50 < E/\text{kcal mol}^{-1} \leq 135$, and $W = 0.2$ for geometries with $E > 135 \text{ kcal mol}^{-1}$ above *c*- SiC_2 . Our fit involves a total of 180 linear coefficients in the polynomial expansion [$L = 11$ in Eq. (8)]; see Tables S1-S4 of the SM to access the numerical coefficients of all parameters resulting from the fit. Figure S2 also portrays some representative cuts of the final analytic CHIPR potential [Eq. (6)] alongside the corresponding *ab initio* ones. Table I displays the stratified rmsd, while Figure 2 shows the distribution of errors of the fitted data set. Accordingly, we note that $\sim 82\%$ of the data is herein fitted with $0.9 \text{ kcal mol}^{-1}$ accuracy. Moreover, Figure 2 indicates that most of the calculated grid points (95% of the total population) are primarily distributed within the $300 \text{ kcal mol}^{-1}$ range above *c*- SiC_2 , thence approximately spanning the energy interval of up to its complete atomization^{62,63} (if we consider the atom+diatom geometries utilized to calibrate the diatomic curves). The high-energy points, particularly those within $300 < E/\text{kcal mol}^{-1} \leq 1200$ (see Table I and Figure 2), are characterized by short CC and/or SiC bond distances which, despite carrying lower weights in the least-squares fitting procedure (see above), are shown to be important to properly model the repulsive walls of the global potential, preventing the three-body term [$V^{(3)}$ in Eq. (6)] from attaining large negative values at these regions.

In relation to our combined CC/MR protocol, we should mention that, despite being extrapolated to the CBS limit, the two *ab initio* theories unavoidably diverge, specially at long distances; a prototypical case is illustrated in Figure 1. This latter is clearly due to single-reference CC which is not expected to properly describe dissociation⁴³. These CC points, whenever present, were eliminated from the fit, warranting a smooth transition between the two data sets and the lowest rmsd; see Figures 1 and S2. In the valence region, correlation energy differences between CC and MR also exist (even at CBS limit) but are less evident (Figure 1), showing the smallest deviations near the global minimum; for example, at *c*- SiC_2 , the CC/CBS and MR/CBS total energies differ by $\sim 71 \mu E_h$, a value that compares quite well with the corresponding estimate of $\sim 11 \mu E_h$ calculated using CCSD(T)-F12b/VQZ-F12 and MRCI(Q)-F12/VQZ-F12 energies. These inherent discrepancies in CC and MR correlation energies are expected to increase when going up in energy, likely attaining larger values at long-range distances (Figure 1). Note, however, that, because the low-energy part of our potential is primarily sampled by CC/CBS points [Figure 3(a)], we expect that the existence of such a CC/MR seam (lying higher in energy) influences little the final spectroscopic properties of the PES to be discussed next.

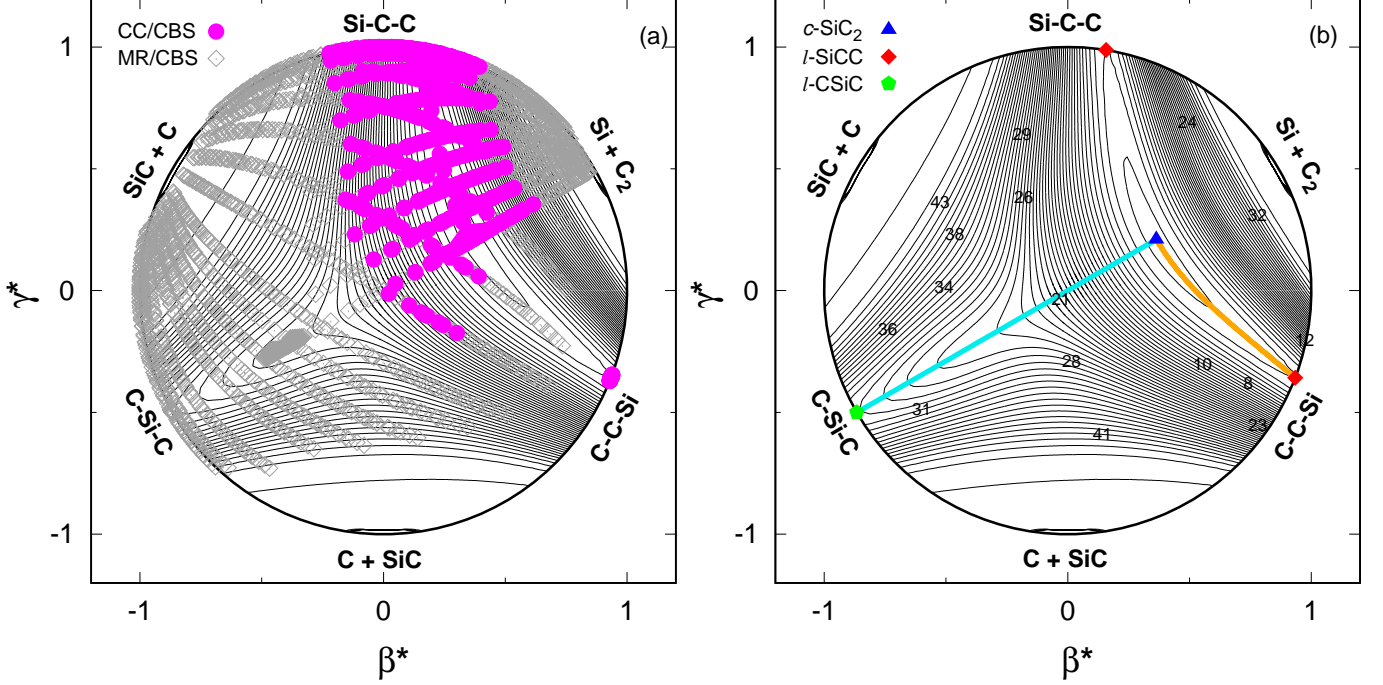


FIG. 3. Relaxed triangular plot in scaled hyperspherical coordinates⁶⁰ [β^* and γ^* ; see Eq. (12)] of the ground-state CHIPR PES of SiC_2 showing (a). the distribution of *ab initio* CCSD(T)/CBS (magenta solid circles) and MRCI(Q)/CBS (gray open diamonds) calibration data set; (b). its global topographical attributes, location of stationary points (indicated by symbols), and isomerization pathways shown later in 1D in Figure 6. In both plots, linear geometries lie at the border of the physical circle, while the C_{2v} line connects $\text{Si}+\text{C}_2$ to $c\text{-SiC}_2$ to $l\text{-CSiC}$. The origin ($\beta^*=0$ and $\gamma^*=0$) defines a D_{3h} configuration and C_s structures are elsewhere. The location of all atom+diatom dissociation channels are properly indicated. Contours are equally spaced by $0.007 E_h$ starting at $-0.5 E_h$. The zero of energy is set relative to the infinitely separated $\text{C}+\text{C}+\text{Si}$ atoms. The corresponding 3D version of plot (b) is shown later in Figure 8.

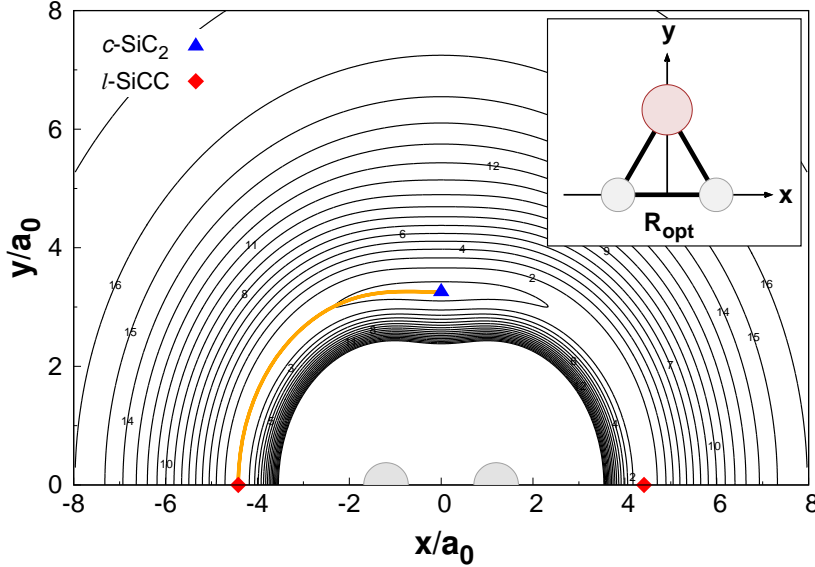


FIG. 4. CHIPR contour plot for a Si atom moving around a partially relaxed C_2 diatom ($2.2 \leq r/a_0 \leq 2.6$), which lies along the x axis with the center of the bond fixed at the origin. x and y coordinates give the position of Si with respect to the origin. Linear geometries are defined by $x \neq 0$ and $y=0$, while the $x=0$ and $y \neq 0$ line describes C_{2v} configurations; C_s structures are elsewhere. Contours are equally spaced by $0.015 E_h$ starting at $-0.5 E_h$. The zero of energy is set relative to the infinitely separated $\text{C}+\text{C}+\text{Si}$ atoms. Solid color line represents the minimum energy path shown in 1D in Figure 6(a).

III. FEATURES OF PES

All major features of the final CHIPR PES are depicted in Figures 3-8. The properties of its stationary points are collected in Table II wherein the most accurate results from the literature^{1,15,17,18,20,21} as well as our own *ab initio* CC and MR values are also included for comparison. Note that, to al-

low for a complete visualization of all topographical attributes of our global CHIPR analytic potential, Figure 3 shows a relaxed-triangular contour plot in scaled hyperspherical coordinates⁶⁰, $\beta^*=\beta/Q$ and $\gamma^*=\gamma/Q$, where

$$\begin{pmatrix} Q \\ \beta \\ \gamma \end{pmatrix} = \begin{pmatrix} 1 & 1 & 1 \\ 0 & \sqrt{3} & -\sqrt{3} \\ 2 & -1 & -1 \end{pmatrix} \begin{pmatrix} R_1^2 \\ R_2^2 \\ R_3^2 \end{pmatrix}, \quad (12)$$

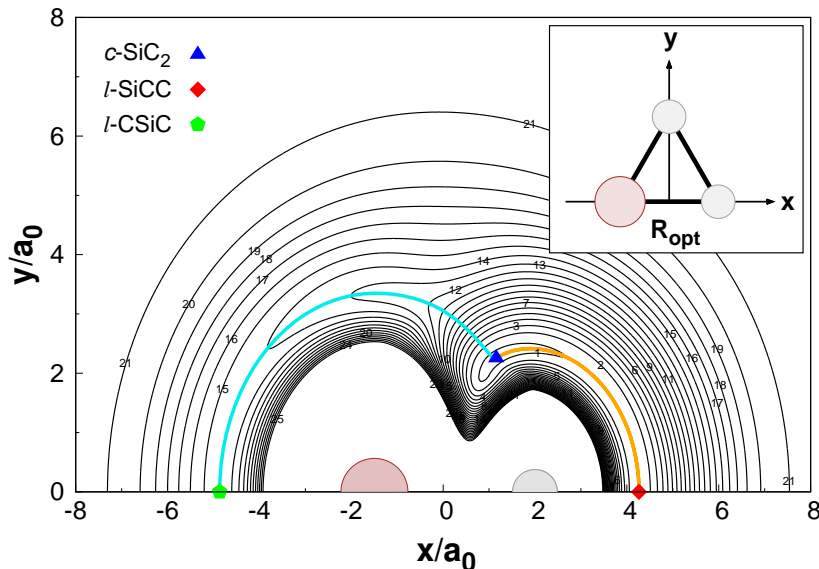


FIG. 5. CHIPR contour plot for a C atom moving around a partially relaxed SiC diatom ($3.0 \leq r/a_0 \leq 4.0$), which lies along the x axis with origin at its center of mass. x and y coordinates define the position of C with respect to the origin. Contours are equally spaced by $0.015 E_h$ starting at $-0.5 E_h$. The zero of energy is set relative to the infinitely separated $C+C+Si$ atoms. Solid color lines represent the minimum energy paths shown in 1D in Figure 6(a) and (b).

and R_1 , R_2 , and R_3 are interatomic distances. Thus, by relaxing the “size” Q of the molecule such as to give the lowest energy for a given “shape” (β and γ) of the triangle formed by the three atoms, the contour plot shown in Figure 3 is then obtained; see legend therein and Refs. 39 and 24 for further details. The corresponding 3D version of this plot is shown later in Figure 8. In turn, Figures 4 and 5 illustrate the PES for the Si and C atoms moving around relaxed C_2 and SiC fragments, respectively. They also summarize in a comprehensive manner all predicted stationary structures from the analytic CHIPR PES to be discussed next.

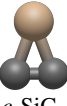
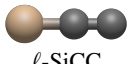

A. Valence region & spectroscopic calculations

According to Figures 3-8, the predicted global minimum on the ground-state singlet PES corresponds to a cyclic C_{2v} geometry, $c\text{-SiC}_2(^1A_1)$. As Table II shows, its characteristic bond lengths and angle are $R_1(\text{Si}-\text{C})=R_2(\text{Si}-\text{C})=3.468 a_0$ and $\alpha(\angle\text{C}-\text{Si}-\text{C})=40.5^\circ$. These values are in excellent agreement with the most reliable theoretical estimates due to Fortenberry *et al.*²⁰ and Koput²¹, differing by less than $0.008 a_0/0.1^\circ$. Recall that these authors include, in addition to CBS energies, contributions from core-core/core-valence electron correlation and scalar relativistic effects in their local PESs; Koput²¹ further accounts for higher-order \mathcal{N} -particle electron correlation beyond CCSD(T). Close agreement is also found between the CHIPR’s $c\text{-SiC}_2$ data and experimental attributes taken from the literature^{1,15,17,18}; see Table II. Indeed, our predicted C–C (ν_1) and Si–C (ν_2) stretching fundamentals reproduce exceedingly well ($\lesssim 3.5 \text{ cm}^{-1}$) the corresponding experimental values¹⁵ and are quite consistent with those calculated from the JK PES (Table II). Yet, larger discrepancies (of up to 16 cm^{-1}) are found for the large-amplitude ν_3 fundamental associated with the internal rotation of the C_2 moiety. As noted elsewhere^{16,21}, the proper description of the expected highly anharmonic potential along this mode [Figures 4 and 6(a)] requires an iterative treatment of the

connected triples (T_3) and quadruples (T_4) correlation contributions in the coupled-cluster expansion; this however would make the task of calculating the global PES of SiC_2 computationally unfeasible, even if limited to a smaller section of PES near $c\text{-SiC}_2$ [Figure 3(a)]. Indeed, the corresponding ν_3 value reported by Koput²¹ differs by less than 3 cm^{-1} from its experimental estimate. Despite the expected lower performance of CHIPR relative to JK in predicting ν_3 , we note that our variationally-computed fundamentals for $c\text{-SiC}_2$ still appear to be slightly more accurate than those reported using the CcCR QFF/VPT2 protocol²⁰, even without considering here relativistic and core-valence correlation effects; see Table II.

To further assess the accuracy of the final CHIPR PES, we have carried out anharmonic vibrational calculations for higher excited modes using the DVR3D software suite⁶⁵ and compared the results with the experimental term energies reported by Ross *et al.*¹⁵. All calculated data are gathered in Table III. Also shown for comparison are the corresponding values reported from the JK local PES²¹. Note that the vibrational band origins cover energies up to about 5200 cm^{-1} (6600 cm^{-1}) above the ground-state zero point level (bottom of the well) of $c\text{-SiC}_2$ and excitations of up to as high as 16 quanta in ν_3 ; the approximate quantum numbers ν_1 and ν_2 refer to the C–C and Si–C stretching vibrations, while ν_3 corresponds to the antisymmetric stretching of the triangular geometry. The results presented in Table III show that our CHIPR PES reproduces remarkably well the vibrational spectrum of $c\text{-SiC}_2$ with a rmsd of 16 cm^{-1} (as expected, the largest deviations are ascribed to overtones and combination bands involving ν_3). This is quite astounding given the global, purely *ab initio* nature of the PES and is clearly an asset of the present dual-level CC/MR protocol³⁹. It should be stressed that such a mixed protocol is herein devised to improve the spectroscopy of global potentials relative to global PESs calibrated solely using MR grid energies. Indeed, our experience shows (see, *e.g.*, Refs. 66 and 25) that purely MR global forms, despite accurately describing the bulk of the PESs, do in general a relatively poor job at reproducing experimental vibrational band

TABLE II. Structural equilibrium parameters (in valence coordinates, R_i in a_0 , α in degrees), harmonic (ω_i) and fundamental (ν_i) frequencies (in cm^{-1}) of the stationary points on the ground-state singlet PES of SiC_2 . Relative energies (ΔE) are in kcal mol^{-1} and given with respect to the C_{2v} global minimum.

Structure	Method ^a	R_1	R_2	α	ΔE^a	ω_1 (ν_1)	ω_2 (ν_2)	ω_3 (ν_3)
 $c\text{-SiC}_2$	CC/AVQZ	3.478	3.478	40.5	0.0	1763.9	807.9	180.5
	MR/AVQZ	3.488	3.488	40.6	0.0	1743.9	793.2	223.2
	CC/CBS ^b				0.0			
	MR/CBS ^b				0.0			
	CcCR QFF ^c	3.460	3.460	40.5		1781.9 (1750.5)	815.1 (844.7)	201.4 (175.4)
	JK PES ^d	3.460	3.460	40.6	0.0	1776.1 (1745.6)	812.7 (837.9)	214.6 (194.1)
	CHIPR PES	3.468	3.468	40.5	0.0	1804.4 (1749.4)	823.2 (840.1)	201.6 (180.4)
	exp.	3.459 ^e	3.459 ^e	40.6 ^e	0.0	1756.8 ^f (1746.0) ^g	844.0 ^f (840.6) ^g	
 $l\text{-SiCC}$	CC/AVQZ	2.434	3.206	180.0	4.8	1887.9	787.4	81.9 i
	MR/AVQZ	2.456	3.231	180.0	4.2	1846.3	765.7	55.7 i
	CC/CBS ^b				5.4			
	MR/CBS ^b				4.5			
	JK PES ^d	2.425	3.192	180.0	5.1	1901.4	790.5	82.6 i
	CHIPR PES	2.430	3.202	180.0	5.4	1893.6	783.5	102.1 i
	exp.				5.4 \pm 0.6 ^h			
 $l\text{-CSiC}$	CC/AVQZ	3.401	3.401	180.0	131.6	947.6	707.5	177.8 i
	MR/AVQZ	3.431	3.431	180.0	128.1	912.3	690.5	162.6 i
	CC/CBS ^b				132.8			
	MR/CBS ^b				129.2			
	CHIPR PES	3.409	3.409	180.0	129.2	902.8	729.2	112.9 i

^a This work unless stated otherwise.

^b CC/CBS and MR/CBS single-point energies calculated at CHIPR PES stationary points.

^c Quartic force field of Ref. 20.

^d Jacek Koput (JK) local PES of Ref. 21.

^e Experimental equilibrium parameters reported in Ref. 20. The corresponding zero-point values are⁶⁴ $R_{1,0} = R_{2,0} = 3.463a_0$ and $\alpha_0 = 40.505^\circ$.

^f Experimental harmonic frequencies taken from Ref. 18.

^g Experimental fundamental frequencies taken from Ref. 15.

^h Potential energy barrier determined by Ross *et al.*¹⁵ from experimental data.

origins of triatomics, showing rmsds of $\sim 50\text{cm}^{-1}$ or even greater. We reiterate that the lower performance of CHIPR when compared to the accurate JK local PES (see Table III) is not surprising given the absence of higher-order effects in our CC calibration data, in addition to the fact that global analytic forms unavoidably entail larger fitting errors, even near the global minimum. In turn and differently from CHIPR, the JK potential cannot physically describe all dissociation channels and may show spurious features at regions of the PES characterized by large C–C bond distances. Additionally, CHIPR describes by built-in the complete atomization of the system. Considering the $c\text{-SiC}_2$'s anharmonic zero point energy (1400.1cm^{-1}) and its stabilization energy relative to the $\text{C}+\text{C}+\text{Si}$ atoms ($-0.474269E_h$), a total atomization energy of $293.6\text{kcal mol}^{-1}$ is predicted from our PES. This value is in excellent agreement with the best theoretical estimate of $293.1\text{kcal mol}^{-1}$ reported by Oyedepo *et al.*⁶³ using the MR-ccCA protocol⁶³ and the early G2 result by Deutsch *et al.*⁶² ($294.7\text{kcal mol}^{-1}$); the last known experimental value is⁶² $301.0 \pm 7\text{kcal mol}^{-1}$.

As Figures 3(b) and 4 portray, $c\text{-SiC}_2$ is connected by two-symmetry equivalent linear ($C_{\infty v}$) transition states, $l\text{-SiCC} (^1\Sigma^+)$, located at $R_1(\text{C} - \text{C}) = 2.430a_0$, $R_2(\text{Si} - \text{C}) = 3.202a_0$ and $\alpha(\angle\text{Si} - \text{C} - \text{C}) = 180.0^\circ$ with an imaginary frequency of 102.1cm^{-1} . The corresponding minimum energy path (MEP) calculated⁶⁷ from the PES is plotted in Figure 6(a) and clearly represents the large-amplitude nearly-free pinwheel motion of C_2 around Si. Indeed, a close look at Figure 6(a) shows that the CHIPR form accurately reproduces the MEP at the CC/CBS level, with the corresponding MR/CBS path being actually lower in energy. Suffice it to say that such MR/CBS points are only shown therein for comparison – they were not included in the fit as this region is only sampled by CC/CBS points (section II A). Our best theoretical estimate (taken from the analytic PES) places $l\text{-SiCC}$ at 5.4kcal mol^{-1} (1886.1cm^{-1}) above $c\text{-SiC}_2$, in excellent agreement with the reported value of 5.1kcal mol^{-1} (1781.9cm^{-1}) by Koput²¹. Most notably, our predicted barrier to linearity is shown to match nearly perfectly the corresponding experimental estimate of¹⁵ $5.4 \pm 0.6\text{kcal mol}^{-1}$.

TABLE III. Calculated and observed vibrational term values (in cm^{-1}) for $c\text{-SiC}_2(^1A_1)$.

ν_1	ν_2	ν_3	Γ_{vib}	Obs ^a	Calc	
					CHIPR ^b	JK ^c
0	0	0	A_1	0.0	0.0	0.0
0	0	2	A_1	352.85	326.1	349.6
0	0	4	A_1	605.33	573.5	600.3
0	0	6	A_1	814.87	793.4	809.2
0	1	0	A_1	840.6	840.1	837.9
0	0	8	A_1	1013.5	997.6	1005.1
0	0	10	A_1	1185.	1179.7	1179.2
0	1	2	A_1	1264.6	1239.0	1261.6
0	0	12	A_1	1350.48	1347.4	1342.6
0	0	14	A_1	1492.16	1490.4	1482.8
0	1	4	A_1	1556.7	1521.9	1549.0
0	0	16	A_1	1614.	1625.5	1609.3
0	2	0	A_1	1667.8	1667.7	1665.2
1	0	0	A_1	1746.0	1749.4	1745.6
1	0	2	A_1	2078.	2054.9	2075.1
1	0	4	A_1	2322.1	2297.4	2318.8
0	3	0	A_1	2465.7	2450.3	2460.4
1	0	6	A_1	2539.	2521.6	2530.7
1	1	0	A_1	2579.2	2588.8	2580.0
1	0	8	A_1	2735.	2733.6	2732.6
1	0	10	A_1	2918.	2924.9	2916.1
0	4	0	A_1	3303.	3292.4	3303.8
1	2	0	A_1	3406.6	3414.9	3405.6
2	0	0	A_1	3465.8	3464.2	3467.1
2	1	0	A_1	4299.	4304.2	4299.7
2	2	0	A_1	5122.	5125.0	5120.6
3	0	0	A_1	5164.	5155.5	5163.4
0	0	1	B_1	196.37	180.4	194.1
0	0	3	B_1	487.2	454.9	482.6
0	0	5	B_1	717.6	686.7	709.7
0	1	1	B_1	917.7	898.0	910.4
0	0	7	B_1	1072.2	1060.7	1070.1
0	0	9	B_1	1107.3	1094.8	1100.1
0	1	3	B_1	1271.	1266.1	1262.8
0	0	11	B_1	1412.	1385.5	1404.8
0	0	13	B_1	1436.5	1425.7	1429.7
0	1	5	B_1	1558.	1561.0	1550.2
0	0	15	B_1	1689.6	1686.1	1677.6
0	1	7	B_1	1883.	1879.9	1877.6
1	0	1	B_1	1925.	1917.5	1928.3
0	2	1	B_1	1955.	1941.3	1955.6
1	0	3	B_1	2201.	2179.3	2202.7
1	0	5	B_1	2430.	2421.7	2428.8
1	0	7	B_1	2627.	2628.8	2634.2
rmsd ^d					16.0	5.3

^a Experimental data from Ref. 15.

^b Calculated using CHIPR PES and DVR3D⁶⁵. The zero point energy is 1400.1cm^{-1} .

^c Jacek Koput (JK) local PES. Data from Ref. 21.

^d Root-mean-square deviations with respect to experimental data.

($1883 \pm 200\text{cm}^{-1}$). These results provide compelling evidence that, at this level, CC appears to be more reliable in describing the $c\text{-SiC}_2/\ell\text{-SiCC}$ region, despite lying at the threshold of single-reference description with^{44,45} $T_1 \sim 0.02$ and $D_1 \sim 0.05$; see inset of Figure 6(a). The corresponding barrier

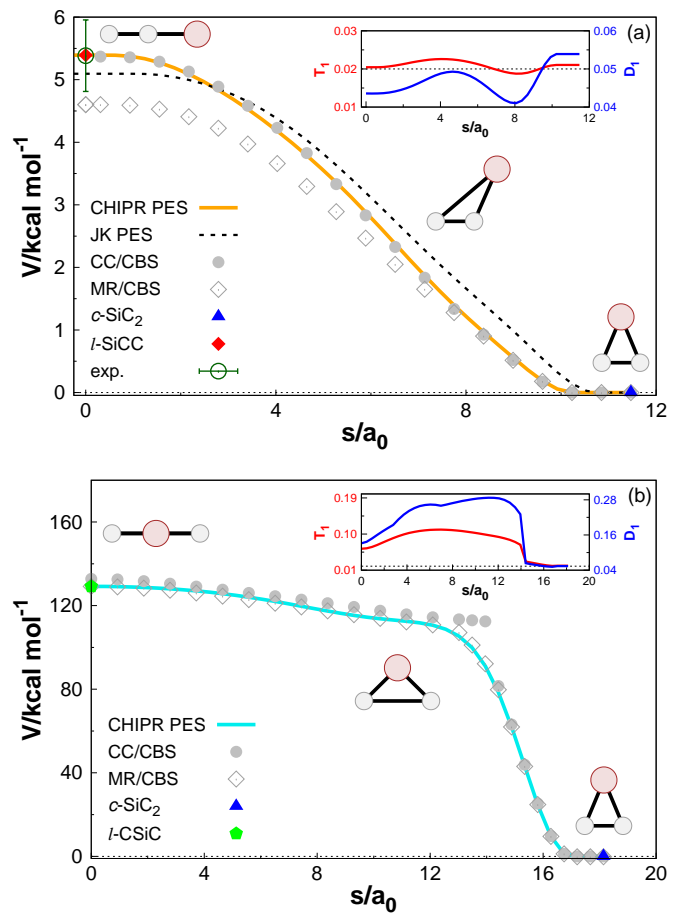


FIG. 6. CHIPR minimum energy paths (s are reaction coordinates in mass-scaled a.u.) and potential energy barriers for the conversion of $c\text{-SiC}_2$ to (a). $\ell\text{-SiCC}$ and (b). $\ell\text{-CSiC}$ configurations. Solid circles and open diamonds indicate *ab initio* CCSD(T)/CBS and MRCI(Q)/CBS single-point energies calculated at the predicted CHIPR geometries. In panel (a), the corresponding path obtained using the Jacek Koput (JK) local PES²¹ as well as the experimentally-derived $c\text{-SiC}_2 \rightarrow \ell\text{-SiCC}$ barrier reported by Ross *et al.*¹⁵ are also shown for comparison. In panels (a) and (b), MRCI(Q)/CBS and CCSD(T)/CBS points, respectively, were not included in the fit and are only plotted for comparison. The insets display the evolution of the coupled-cluster T_1 and D_1 diagnostics along the underlying paths as obtained from CCSD(T)/AV5Z calculations.

predicted at MR/CC level is $\approx 0.9\text{kcal mol}^{-1}$ lower than the CC/CBS estimate (Table II), being nearly coincident with the value of 4.5kcal mol^{-1} reported by Koput at MR-ACPF/cc-pV6Z level²¹.

A notable aspect of the CHIPR PES, discussed previously in early studies^{31–33}, is the existence of an auxiliary $D_{\infty h}$ transition state, $\ell\text{-CSiC}(^1\Sigma_g^+)$. As Table II shows, this linear form has characteristic bond lengths of $R_1(\text{Si}-\text{C}) = R_2(\text{Si}-\text{C}) = 3.409a_0$ and an imaginary frequency of 112.9cm^{-1} along the bending coordinate. Its connection to $c\text{-SiC}_2$ is perhaps best seen from the contour plots in Figures 3(b) and 5; see the cyan solid lines represented therein. The associated isomerization pathway⁶⁷ in 1D is presented in Figure 6(b), wherein the major topographical valence attributes of the CHIPR PES across C_{2v} geometries can be assessed. Accordingly, $\ell\text{-CSiC}$ is predicted from our final CHIPR form to lie $129.2\text{kcal mol}^{-1}$

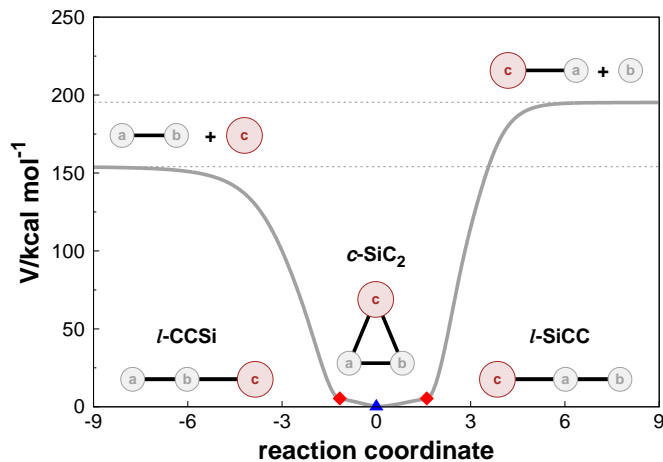


FIG. 7. 1D cut of the CHIPR PES along the minimum energy path connecting C_2+Si and $SiC+C$ via SiC_2 intermediates. Black dashed lines mark the associated energies of the infinitely separated atom+diatom fragments. The a, b, c labels are introduced to distinguish between symmetry-equivalent structures.

above $c-SiC_2$. Differently from $\ell-SiCC$ which span a low energy region of the PES primarily sampled by CC/CBS points [Figures 3(a)], the description of $\ell-CSiC$ and vicinities can only be accurately done at MR/CBS level. In fact, as the inset of Figure 6(b) shows, at this region of the nuclear configuration space the predicted CC diagnostics [e.g., $T_1 \approx 0.11$ and $D_1 \approx 0.27$ halfway through the MEP] far exceed the accepted limiting values: $T_1 \lesssim 0.02^{44}$, $D_1 \lesssim 0.05^{45}$, thus clearly entailing a multi-reference approach. This is explained by the presence of several low-lying excited electronic states in this region, as Figure S3(a) illustrates. Indeed, Figure 6(b) evinces that the CHIPR form mimics excellently well the *ab initio* MR/CBS data, with the predicted barrier to linearity matching exactly the one calculated at this level (Table II). We further note that, in Figure 6(b), the CC/CBS data shown are only plotted for comparison; they were not included in the calibration data set as this high-energy valence region of the PES (with $s \lesssim 15 a_0$) is sampled solely by MR/CBS calculations.

B. Proof of concept: long-range region & reaction dynamics calculations

Apart from accurately modeling the valence (strongly-bound) chemical space, the contour plots shown in Figures 3–5 evidently pinpoint the reliability of the CHIPR form to describe long-range and dissociation features of the SiC_2 PES, in addition to naturally reflect its correct permutational symmetry. This is clearly an asset of the CHIPR^{34–37} formalism [namely, Eq. (8)] and is the major deliverable of the present work. Figure 7 shows the calculated MEP for the chemical conversion of C_2+Si to $SiC+C$ that proceeds via SiC_2 intermediates. Accordingly, both forward and reverse collision processes evolve without activation barriers for collinear atom-diatom approaches, leading directly to the formation of $\ell-SiCC$. This structure is subsequently converted to $c-$

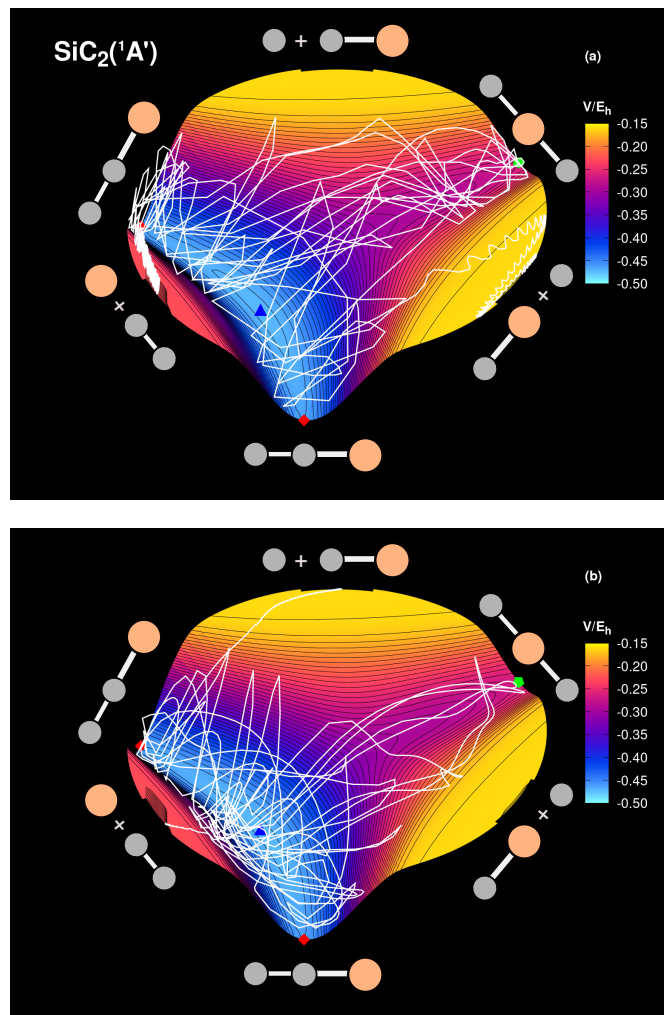


FIG. 8. Relaxed 3D hyperspherical plots [see also Figure 3(b)] of the CHIPR PES of $SiC_2(^1A')$ showing the time evolution (in coordinate space) of sample reactive quasi-classical trajectories (solid white lines) calculated using the VENUS96C code⁶⁸ for $Si(^3P) + C_2(^3\Pi_u) \rightarrow SiC(X^3\Pi) + C(^3P)$ with distinct initial conditions (a), vibrationally excited $C_2(v=11)$ and collision energy of $1.0 \text{ kcal mol}^{-1}$ and (b), ground-state C_2 and collision energy of $42.0 \text{ kcal mol}^{-1}$. Stationary points and coordinates as in Figure 3(b). The zero of energy is set relative to the infinitely separated $C+C+Si$ atoms.

SiC_2 by way of low-energy (nearly-free) C_2 internal rotations [Figure 6(a)]; the stabilization energy of the $c-SiC_2$ complex is predicted to be *ca.* -154.1 and $-195.4 \text{ kcal mol}^{-1}$ relative to the infinitely separated C_2+Si and $SiC+C$ fragments, respectively, this former being quite close to the value of $-152.9 \text{ kcal mol}^{-1}$ reported by Nielsen *et al.*¹⁶ based on high-level focal point thermochemical analyses. Indeed, as Figure 7 shows, the $C_2+Si \rightarrow SiC+C$ reaction is highly endothermic ($40.4 \text{ kcal mol}^{-1}$, including the zero-point energies of the reactants and products) which makes this process feasible only in high-temperature environments, e.g., in the inner envelopes surrounding (late-type) carbon-rich stars^{10,12}, thence conceivably playing therein a key role in the formation of gas-phase SiC , and consequently solid SiC dust. Initial assessments indicate that, in order to effectively initiate such a reaction, C_2

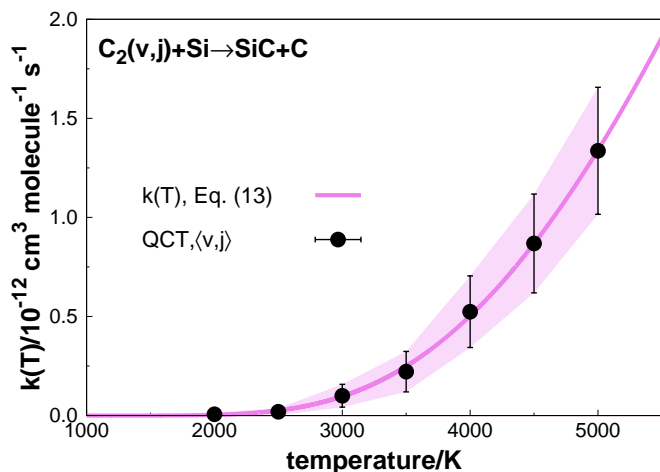


FIG. 9. Calculated rate constants and associated error bars for the $\text{Si}(^3P) + \text{C}_2(^3\Pi_u) \rightarrow \text{SiC}(X^3\Pi) + \text{C}(^3P)$ reaction within the temperature range of $2000 \leq T/\text{K} \leq 5000$. The lines show the predicted QCT thermally averaged results from Eq. (13). For clarity, the QCT results are shown with 99.6% (3σ) error bars.

must be initially pumped⁶⁹ to higher vibrational states (up to at least $v = 10$ -11) or collide with a high-energy Si atom, with relative translational energies of the order of $\sim 41 \text{ kcal mol}^{-1}$ or higher; see, *e.g.*, Figure 8. These conditions can be fulfilled within the inner layers of the circumstellar shells of evolved C-stars (*e.g.*, IRC+10216) characterized by temperatures of ~ 1000 -3000 K or higher and where $\text{C}_2(X^1\Sigma_g^+, a^3\Pi_u)$ and other silicon-carbon species are known to be particularly conspicuous¹². To further assess the reliability of such a reaction, we have run preliminary quasi-classical trajectory (QCT) calculations^{68,70} on the CHIPR PES using a locally modified version of the VENUS96C code⁶⁸; for a thorough description of the methodology here utilized, see Ref. 71 and Table S5. At the high temperature regime considered ($2000 \leq T/\text{K} \leq 5000$), the calculated thermal rate coefficients for $\text{C}_2 + \text{Si} \rightarrow \text{SiC} + \text{C}$ can be accurately represented by the Arrhenius-Kooij formula⁷²:

$$k(T) = A \left(\frac{T}{300} \right)^B \exp \left(\frac{-C}{T} \right), \quad (13)$$

where $A = 1.22582 \times 10^{-10} \text{ cm}^3 \text{ molecule}^{-1} \text{ s}^{-1}$, $B = -0.161897$, and $C = 20305.15 \text{ K}$. This is plotted in Figure 9, together with the calculated QCT data which are numerically defined in Table S5. Accordingly, the theoretically-predicted rate constants for $\text{C}_2 + \text{Si} \rightarrow \text{SiC} + \text{C}$ show a positive temperature dependence, increasing steeply from $T = 3000 \text{ K}$. This provides compelling evidence for its relevance in the gas-phase synthesis of SiC and related solid SiC dust formation in the innermost envelopes of C-stars⁷³. Further investigations in this direction are in order and a detailed account of the overall $\text{C}_2 + \text{Si} \rightarrow \text{SiC} + \text{C}$ dynamics and kinetics undoubtedly requires a careful assessment of the possible contributions of other excited-states PESs correlating to the same reactant/product channels; this is clearly beyond the scope of our present preliminary analysis and will be the focus of future studies. Also of relevance is the reverse

(barrierless and exothermic) $\text{SiC} + \text{C} \rightarrow \text{C}_2 + \text{Si}$ reaction (Figure 7) which, differently from $\text{C}_2 + \text{Si} \rightarrow \text{SiC} + \text{C}$, surely occurs at cold and ultracold temperatures, hence dominated by long-range forces; indeed, the expected high reactivity of SiC with⁷⁴ atomic C and O at low T s may help explain the lack of SiC detections in cold interstellar environments⁷⁵⁻⁷⁷.

IV. CONCLUSIONS

We report the first global PES for ground-state $\text{SiC}_2(^1A')$ based on CBS extrapolated *ab initio* energies and the CHIPR method for the analytical modeling. By relying on a mixed CCSD(T) and MRCI(Q) protocol, we ensure that the final potential recovers much of the spectroscopy of its cyclic global minimum, while still permitting an accurate description of isomerization and fragmentation processes, all with the correct permutational symmetry as naturally warranted by CHIPR. Bound-state calculations performed anew have shown that the present purely-*ab initio* CHIPR PES is capable of reproducing the experimental vibrational spectrum of cyclic SiC_2 with a rmsd of 16 cm^{-1} . Despite not outperforming the spectroscopic quality of the most accurate local PES to date²¹, our proposed dual-level CCSD(T)/MRCI(Q) CBS protocol is expected to improve the spectroscopy of global ground-state PESs when compared with purely MRCI(Q)-based global forms. Further improvements can be so envisaged by either fine-tuning the theoretically-predicted potential parameters with input experimental information^{66,78} or morphing the original global form with a spectroscopically-accurate local potential²⁵. Aside from anharmonic vibrational calculations, the global nature of our CHIPR PES is further exploited by performing preliminary quasi-classical trajectory calculations for the $\text{C}_2 + \text{Si} \rightarrow \text{SiC} + \text{C}$ endothermic reaction. The calculated thermal rate coefficients within the temperature range of $2000 \leq T/\text{K} \leq 5000$ hint for its prominence in the gas-phase synthesis of SiC and, presumably, SiC dust formation in the inner envelopes surrounding carbon-rich stars^{10,12}.

SUPPLEMENTARY MATERIAL

See the supplementary material to assess the performance of the PES alongside *ab initio* grid data, the numerical coefficients of the final CHIPR analytic form as well as the calculated QCT reaction rate coefficients.

ACKNOWLEDGMENTS

This work has received funding from the European Union's Horizon 2020 research and innovation program under the Marie Skłodowska-Curie grant agreement no 894321. CMRR thanks also the Academic Leiden Interdisciplinary Cluster Environment (ALICE) provided by Leiden University for the computational resources. AJCV thanks the support of China's Shandong Province "Double-Hundred Talent Plan" (2018), Coordenação de Aperfeiçoamento de Pessoal de Nível

Superior-Brasil (CAPES)-Finance Code 001, Conselho Nacional de Desenvolvimento Científico e Tecnológico (CNPq), and Foundation for Science and Technology, Portugal, in the framework of the project 55UIDB/00313/2020.

AUTHOR DECLARATIONS

Conflict of Interest

The authors have no conflicts to disclose.

DATA AVAILABILITY STATEMENT

The full set of *ab initio* grid points supporting the findings of this study is available from the corresponding author upon reasonable request. A Fortran subroutine of the final CHIPR PES that readily evaluates the potential and gradient at any arbitrary geometry is made available as supplementary material.

- ¹P. Thaddeus, S. E. Cummins, and R. A. Linke, "Identification of the SiCC Radical Toward IRC+10216: The First Molecular Ring in an Astronomical Source," *ApJ* **283**, L45–L48 (1984).
- ²L. A. Nyman, H. Olofsson, L. E. B. Johansson, R. S. Booth, U. Carlstrom, and R. Wolstencroft, "A Molecular Radio Line Survey of the Carbon Star IRAS 15194-5115," *A&A* **269**, 377–389 (1993).
- ³P. D. Gensheimer and L. E. Snyder, "A Search for Vibrationally Excited SiC₂ v₃=1 toward IRC+10216," *ApJ* **490**, 819–822 (1997).
- ⁴P. J. Sarre, M. E. Hurst, and T. Lloyd Evans, "SiC₂ in Carbon Stars: Merrill-Sanford Absorption Bands Between 4100 and 5500 Å," *MNRAS* **319**, 103–110 (2000).
- ⁵D. H. Morgan, D. Hatzidimitriou, and R. D. Cannon, "Merrill-Sanford Bands in Large Magellanic Cloud Carbon Stars," *MNRAS* **355**, 1196–1206 (2004).
- ⁶J. Cernicharo, L. B. F. M. Waters, L. Decin, P. Encrenaz, A. G. G. M. Tielens, M. Agúndez, E. De Beck, H. S. P. Müller, J. R. Goicoechea, M. J. Barlow, A. Benz, N. Crimier, F. Daniel, A. M. Di Giorgio, M. Fich, T. Gaier, P. García-Lario, A. de Koter, T. Khouri, R. Liseau, R. Lombaert, N. Erickson, J. R. Pardo, J. C. Pearson, R. Shipman, C. Sánchez Contreras, and D. Teyssier, "A High-Resolution Line Survey of IRC+10216 with Herschel/HIFI- First Results: Detection of Warm Silicon Dicarbide (SiC₂)," *A&A* **521**, L8 (2010).
- ⁷D. L. Kokkin, S. Brünken, K. H. Young, N. A. Patel, C. A. Gottlieb, P. Thaddeus, and M. C. McCarthy, "The Rotational Spectra of ²⁹SiC₂ and ³⁰SiC₂," *ApJS* **196**, 17 (2011).
- ⁸H. S. P. Müller, J. Cernicharo, M. Agúndez, L. Decin, P. Encrenaz, J. Pearson, D. Teyssier, and L. Waters, "Spectroscopic Parameters for Silacyclopentynylidene, SiC₂, from Extensive Astronomical Observations Toward CW Leo (IRC+10216) with the Herschel Satellite," *J. Mol. Spectrosc.* **271**, 50–55 (2012).
- ⁹D. Gobrecht, S. Cristallo, L. Piersanti, and S. T. Bromley, "Nucleation of Small Silicon Carbide Dust Clusters in AGB Stars," *ApJ* **840**, 117 (2017).
- ¹⁰S. Massalkhi, M. Agúndez, J. Cernicharo, L. Velilla Prieto, J. R. Goicoechea, G. Quintana-Lacaci, J. P. Fonfría, J. Alcolea, and V. Bujarbal, "Abundance of SiC₂ in Carbon Star Envelopes - Evidence that SiC₂ is a Gas-Phase Precursor of SiC Dust," *A&A* **611**, A29 (2018).
- ¹¹J. Cernicharo, M. Guélin, M. Agúndez, J. R. Pardo, S. Massalkhi, J. P. Fonfría, L. Velilla Prieto, G. Quintana-Lacaci, N. Marcelino, C. Marka, S. Navarro, and C. Kramer, "IRC+10216 as a Spectroscopic Laboratory: Improved Rotational Constants for SiC₂, Its Isotopologues, and Si₂C," *A&A* **618**, A4 (2018).
- ¹²M. C. McCarthy, C. A. Gottlieb, and J. Cernicharo, "Building Blocks of Dust: A Coordinated Laboratory and Astronomical Study of the Archtype AGB Carbon Star IRC+10216," *J. Mol. Spectrosc.* **356**, 7–20 (2019).
- ¹³M. Agúndez, J. I. Martínez, P. L. de Andres, J. Cernicharo, and J. A. Martín-Gago, "Chemical Equilibrium in AGB Atmospheres: Successes, Failures, and Prospects for Small Molecules, Clusters, and Condensates," *A&A* **637**, A59 (2020).
- ¹⁴M. K. Sharma and A. K. Sharma, "Investigation of Silicon Dicarbide (SiC₂) in Circumstellar Envelopes Around Carbon-Rich AGB Stars," *Indian J. Phys.* **94**, 1869–1874 (2020).
- ¹⁵S. C. Ross, T. J. Butenhoff, E. A. Rohlfing, and C. M. Rohlfing, "SiC₂: A Molecular Pinwheel," *J. Chem. Phys.* **100**, 4110–4126 (1994).
- ¹⁶I. M. B. Nielsen, W. D. Allen, A. G. Császár, and H. F. Schaefer, "Toward Resolution of the Silicon Dicarbide (SiC₂) Saga: *Ab Initio* Excursions in the Web of Polytopism," *J. Chem. Phys.* **107**, 1195–1211 (1997).
- ¹⁷D. L. Michalopoulos, M. E. Geusic, P. R. R. Langridge-Smith, and R. E. Smalley, "Visible Spectroscopy of Jet-Cooled SiC₂: Geometry and Electronic Structure," *J. Chem. Phys.* **80**, 3556–3560 (1984).
- ¹⁸T. J. Butenhoff and E. A. Rohlfing, "Laser-Induced Fluorescence Spectroscopy of Jet-Cooled SiC₂," *J. Chem. Phys.* **95**, 1–8 (1991).
- ¹⁹J. P. Kenny, W. D. Allen, and H. F. Schaefer, "Complete Basis Set Limit Studies of Conventional and R12 Correlation Methods: The Silicon Dicarbide (SiC₂) Barrier to Linearity," *J. Chem. Phys.* **118**, 7353–7365 (2003).
- ²⁰R. C. Fortenberry, T. J. Lee, and H. S. Müller, "Excited Vibrational Level Rotational Constants for SiC₂: A Sensitive Molecular Diagnostic for Astrophysical Conditions," *Mol. Astrophys.* **1**, 13–19 (2015).
- ²¹J. Koput, "Ab Initio Potential Energy Surface and Vibration-Rotation Energy Levels of Silicon Dicarbide, SiC₂," *J. Comp. Chem.* **37**, 2395–2402 (2016).
- ²²J. Oddershede, J. R. Sabin, G. H. F. Dierksen, and N. E. Grüner, "The Structure and Spectrum of SiC₂," *J. Chem. Phys.* **83**, 1702–1708 (1985).
- ²³E. Clementi, H. Kistenmacher, and H. Popkie, "Study of the Electronic Structure of Molecules. XVIII. Interaction Between a Lithium Atom and a Cyano Group as an Example of a Polytopic Bond," *J. Chem. Phys.* **58**, 2460–2466 (1973).
- ²⁴C. M. R. Rocha and A. J. C. Varandas, "Accurate *Ab Initio*-Based Double Many-Body Expansion Potential Energy Surface for the Adiabatic Ground-State of the C₃ Radical Including Combined Jahn-Teller plus Pseudo-Jahn-Teller Interactions," *J. Chem. Phys.* **143**, 074302–074318 (2015).
- ²⁵C. M. R. Rocha and A. J. C. Varandas, "Energy-Switching Potential Energy Surface for Ground-State C₃," *Chem. Phys. Lett.* **700**, 36–43 (2018).
- ²⁶C. A. Gottlieb, J. M. Vrtilek, and P. Thaddeus, "Laboratory Measurement of the Rotational Spectrum of SiCC," *ApJL* **343**, L29 (1989).
- ²⁷R. A. Shepherd and W. R. M. Graham, "FTIR Matrix Isolation Study of Carbon-13 Substituted SiC₂," *J. Chem. Phys.* **82**, 4788–4790 (1985).
- ²⁸J. D. Presilla-Márquez, W. R. M. Graham, and R. A. Shepherd, "Fourier Transform Far Infrared Spectroscopy of the v₃ Vibration of SiC₂ in Ar at 10 K," *J. Chem. Phys.* **93**, 5424–5428 (1990).
- ²⁹M. Izuha, S. Yamamoto, and S. Saito, "Rotational Spectrum of SiC₂ in the v₃ Excited State," *Spectrochim. Acta A Mol. Biomol. Spectrosc.* **50**, 1371–1378 (1994).
- ³⁰Q. Zhang, D.-P. Zhang, B.-X. Zhu, J.-W. Gu, C.-T. Yu, Z.-J. Xiao, Y. Chen, and D.-F. Zhao, "High-Resolution Spectroscopy of the 0₀⁰, 2₀¹, 3₀¹ and 3₁¹ Bands in the $\tilde{A}^1B_2-\tilde{X}^1A_1$ Transition of SiC₂," *J. Mol. Spectrosc.* **372**, 111306 (2020).
- ³¹S. Green, "Theoretical Study of Silicon Dicarbide," *ApJ* **266**, 895–901 (1983).
- ³²S. Arulmozhiraja and P. Kolandaivel, "Four Energetically Low Lying States of SiC₂," *J. Mol. Struct. THEOCHEM* **334**, 71–79 (1995).
- ³³Y. Zhang, C.-Y. Zhao, W.-H. Fang, and Z.-H. Lu, "High Accuracy Studies on the Ground State and Transition State of SiC₂," *J. Mol. Struct. THEOCHEM* **454**, 31–40 (1998).
- ³⁴A. J. C. Varandas, "Combined-Hyperbolic-Inverse-Power-Representation of Potential Energy Surfaces: A Preliminary Assessment for H₃ and HO₂," *J. Chem. Phys.* **138**, 054120–054133 (2013).
- ³⁵A. J. C. Varandas, "Putting Together the Pieces: A Global Description of Valence and Long-Range Forces via Combined Hyperbolic Inverse Power Representation of the Potential Energy Surface," in *Reaction Rate Constant Computations: Theories and Applications*, edited by K. Han and T. Chu (The Royal Society of Chemistry, 2013) Chap. 17, pp. 408–445.
- ³⁶C. M. R. Rocha and A. J. C. Varandas, "A General Code for Fitting Global Potential Energy Surfaces via CHIPR Method: Triatomic Molecules," *Comput. Phys. Commun.* **247**, 106913 (2020).

- ³⁷C. M. R. Rocha and A. J. C. Varandas, "A General Code for Fitting Global Potential Energy Surfaces via CHIPR Method: Direct-Fit Diatomic and Tetratomic Molecules," *Comput. Phys. Commun.* **258**, 107556 (2021).
- ³⁸H. J. Werner, P. J. Knowles, G. Knizia, F. R. Manby, M. Schütz, and *et al.*, "MOLPRO, a package of *ab initio* programs, version 2010.1," (2010), see: <http://www.molpro.net>, Cardiff, U.K., 2010.
- ³⁹B. R. L. Galvão and A. J. C. Varandas, "Accurate Double Many-Body Expansion Potential Energy Surface for $N_3(^4A'')$ from Correlation Scaled *Ab Initio* Energies with Extrapolation to the Complete Basis Set Limit," *J. Phys. Chem. A* **113**, 14424–14430 (2009).
- ⁴⁰P. J. Knowles, C. Hampel, and H. Werner, "Coupled Cluster Theory for High Spin, Open Shell Reference Wave Functions," *J. Chem. Phys.* **99**, 5219–5227 (1993).
- ⁴¹P. Piecuch, M. Wloch, and A. J. C. Varandas, "Renormalized Coupled-Cluster Methods: Theoretical Foundations and Application to the Potential Function of Water," in *Topics in the Theory Of Chemical and Physical Systems*, edited by S. Lahmar, J. Maruani, S. Wilson, and G. Delgado-Barrio (Springer Netherlands, Dordrecht, 2007) pp. 63–121.
- ⁴²R. J. Bartlett and M. Musiał, "Coupled-Cluster Theory in Quantum Chemistry," *Rev. Mod. Phys.* **79**, 291–352 (2007).
- ⁴³P. G. Szalay, T. Müller, G. Gidofalvi, H. Lischka, and R. Shepard, "Multiconfiguration Self-Consistent Field and Multireference Configuration Interaction Methods and Applications," *Chem. Rev.* **112**, 108–181 (2012).
- ⁴⁴T. J. Lee and P. R. Taylor, "A Diagnostic for Determining the Quality of Single-Reference Electron Correlation Methods," *Int. J. Quantum Chem.* **36**, 199–207 (1989).
- ⁴⁵C. L. Janssen and I. Nielsen, "New Diagnostics for Coupled-Cluster and Møller-Plesset Perturbation Theory," *Chem. Phys. Lett.* **290**, 423–430 (1998).
- ⁴⁶A. J. C. Varandas, "Straightening the Hierarchical Staircase for Basis Set Extrapolations: A Low-Cost Approach to High-Accuracy Computational Chemistry," *Annu. Rev. Chem.* **69**, 177–203 (2018).
- ⁴⁷A. J. C. Varandas, "Extrapolation in quantum chemistry: Insights on energetics and reaction dynamics," *J. Theor. Comp. Chem.* **19**, 2030001 (2020).
- ⁴⁸T. H. Dunning, "Gaussian Basis Sets for Use in Correlated Molecular Calculations. I. The Atoms Boron through Neon and Hydrogen," *J. Chem. Phys.* **90**, 1007–1023 (1989).
- ⁴⁹R. A. Kendall, T. H. Dunning, and R. J. Harrison, "Electron Affinities of the First-Row Atoms Revisited. Systematic Basis Sets and Wave Functions," *J. Chem. Phys.* **96**, 6796–6806 (1992).
- ⁵⁰C. M. R. Rocha and A. J. C. Varandas, "A Global CHIPR Potential Energy Surface for Ground-State C_3H and Exploratory Dynamics Studies of Reaction $C_2+CH\rightarrow C_3+H$," *Phys. Chem. Chem. Phys.* **21**, 24406–24418 (2019).
- ⁵¹F. N. N. Pansini, A. C. Neto, and A. J. C. Varandas, "Extrapolation of Hartree-Fock and Multiconfiguration Self-Consistent-Field Energies to the Complete Basis Set Limit," *Theo. Chem. Acc.* **135**, 261–267 (2016).
- ⁵²A. J. C. Varandas and F. N. N. Pansini, "Narrowing the Error in Electron Correlation Calculations by Basis Set Re-hierarchization and Use of the Unified Singlet and Triplet Electron-Pair Extrapolation Scheme: Application to a Test Set of 106 Systems," *J. Chem. Phys.* **141**, 224113–224121 (2014).
- ⁵³F. N. N. Pansini, A. C. Neto, and A. J. C. Varandas, "On the Performance of Various Hierarchized Bases in Extrapolating the Correlation Energy to the Complete Basis Set Limit," *Chem. Phys. Lett.* **641**, 90–96 (2015).
- ⁵⁴C. M. R. Rocha and A. J. C. Varandas, "Accurate CHIPR Potential Energy Surface for the Lowest Triplet State of C_3 ," *J. Phys. Chem. A* **123**, 8154–8169 (2019).
- ⁵⁵A. J. C. Varandas, "Extrapolating to the One-Electron Basis-Set Limit in Electronic Structure Calculations," *J. Chem. Phys.* **126**, 244105–244119 (2007).
- ⁵⁶J. N. Murrell, S. Carter, S. C. Farantos, P. Huxley, and A. J. C. Varandas, *Molecular Potential Energy Functions* (John Wiley & Sons, Chichester, 1984).
- ⁵⁷G. Herzberg, *Molecular Spectra and Molecular Structure III. Electronic Spectra and Electronic Structure of Polyatomic Molecules* (Van Nostrand, New York, 1966).
- ⁵⁸A. Kramida, Atomic Energy Levels and Spectra Bibliographic Database (version 2.0). [Online] Available: <https://physics.nist.gov/Elevbib> [October 2, 2018]. National Institute of Standards and Technology, Gaithersburg, MD (2018).
- ⁵⁹K. P. Huber and G. Herzberg, *Molecular Spectra and Molecular Structure IV. Constants of Diatomic Molecules.*, Vol. IV (Van Nostrand, New York, 1979).
- ⁶⁰A. J. C. Varandas, "A Useful Triangular Plot of Triatomic Potential Energy Surfaces," *Chem. Phys. Lett.* **138**, 455–461 (1987).
- ⁶¹A. J. C. Varandas, "Accurate Combined-Hyperbolic-Inverse-Power-Representation of *Ab Initio* Potential Energy Surface for the Hydroperoxyl Radical and Dynamics Study of $O+OH$ Reaction," *J. Chem. Phys.* **138**, 134117–134123 (2013).
- ⁶²P. Deutsch and L. Curtiss, "A Theoretical Study of Triatomic Carbon-Silicon Mixed Clusters. Relative Energies and Binding Energies," *Chem. Phys. Lett.* **226**, 387–391 (1994).
- ⁶³G. A. Oyedepo, C. Peterson, and A. K. Wilson, "Accurate Predictions of the Energetics of Silicon Compounds Using the Multireference Correlation Consistent Composite Approach," *J. Chem. Phys.* **135**, 094103 (2011).
- ⁶⁴M. Bogey, M. Cordonnier, C. Demuynck, and J. L. Destombes, "Millimeter- and Submillimeter-Wave Spectroscopy of Nonrigid Transient Molecules: Analysis of Silane and Acetylene Plasmas," in *Structures and Conformations of Non-Rigid Molecules*, edited by J. Laane, M. Dakkouri, B. van der Veken, and H. Oberhammer (Springer Netherlands, Dordrecht, 1993) pp. 303–323.
- ⁶⁵J. Tennyson, M. A. Kostin, P. Barletta, G. J. Harris, O. L. Polyansky, J. Ramanlal, and N. F. Zobov, "DVR3D: A Program Suite for the Calculation of Rotation-Vibration Spectra of Triatomic Molecules," *Comput. Phys. Commun.* **163**, 85–116 (2004).
- ⁶⁶A. J. C. Varandas and S. P. J. Rodrigues, "A Realistic Double Many-Body Expansion Potential Energy Surface for $SO_2(\tilde{X}^1A')$ from a Multiproperty Fit to Accurate *Ab Initio* Energies and Vibrational Levels," *Spectrochim. Acta Mol. Biomol. Spectrosc.* **58**, 629–647 (2002).
- ⁶⁷J. Zheng, J. L. Bao, D. G. Truhlar, and *et al.*, "Polyrate 17-C, a computer program for the calculation of chemical reaction rates for polyatomics," (2017), see: <https://comp.chem.umn.edu/polyrate/>, University of Minnesota, Minneapolis, MN, 2017.
- ⁶⁸W. L. Hase, R. J. Duchovic, X. Hu, A. Komornik, K. F. Lim, D. H. Lu, G. H. Peslherbe, K. N. Swamy, S. R. V. Linde, A. J. C. Varandas, H. Wang, and R. J. Wolf, "VENUS96: A General Chemical Dynamics Computer Program," *QCPE Bull.* **16**, 43 (1996).
- ⁶⁹A. Zanchet, M. Agúndez, V. J. Herrero, A. Aguado, and O. Roncero, "Sulfur Chemistry in the Interstellar Medium: The Effect of Vibrational Excitation of H_2 in the Reaction $S^++H_2\rightarrow SH^++H$," *ApJ* **146**, 125 (2013).
- ⁷⁰G. H. Peslherbe, H. Wang, and W. L. Hase, "Monte Carlo Sampling for Classical Trajectory Simulations," in *Adv. Chem. Phys.* (Wiley-Blackwell, 1999) Chap. 6, pp. 171–201.
- ⁷¹C. M. R. Rocha and H. Linnartz, "Theoretical Studies of Carbon Fractionation in Reactions of C with C_2 : Dynamics, Kinetics and Isotopologue Equilibria," *A&A* **647**, A142 (2021).
- ⁷²K. J. Laidler, "The Development of the Arrhenius Equation," *J. Chem. Educ.* **61**, 494–498 (1984).
- ⁷³J. Cernicharo, C. A. Gottlieb, M. Guelin, P. Thaddeus, and J. M. Vrtilek, "Astronomical and Laboratory Detection of the SiC Radical," *ApJL* **341**, L25 (1989).
- ⁷⁴D. D. S. Mackay, "SiO in Dense Molecular Clouds Reconsidered," *MNRAS* **278**, 62–72 (1996).
- ⁷⁵E. Herbst, T. J. Millar, S. Wlodek, and D. K. Bohme, "The Chemistry of Silicon in Dense Interstellar Clouds," *A&A* **222**, 205–210 (1989).
- ⁷⁶D. C. B. Whittet, W. W. Duley, and P. G. Martin, "On the Abundance of Silicon Carbide in the Interstellar Medium," *MNRAS* **244**, 427 (1990).
- ⁷⁷T. Chen, C. Y. Xiao, A. Li, and C. T. Zhou, "Where Have All the Interstellar Silicon Carbides Gone?" *MNRAS* **509**, 5231–5236 (2021).
- ⁷⁸A. J. C. Varandas and S. P. J. Rodrigues, "New Double Many-Body Expansion Potential Energy Surface for Ground-State HCN from a Multiproperty Fit to Accurate *Ab Initio* Energies and Rovibrational Calculations," *J. Phys. Chem. A* **110**, 485–493 (2006).